Relation between electrical properties and microstructure of $YBa_2Cu_3O_{7-x}$ thin films deposited by single-target off-axis sputtering

A. C. Westerheim,[a] Alfredo C. Anderson, and D. E. Oates
Lincoln Laboratory, Massachusetts Institute of Technology, Lexington, Massachusetts 02173-9108

S. N. Basu and D. Bhatt
Department of Manufacturing Engineering, Boston University, Boston, Massachusetts 02215

M. J. Cima
Department of Materials Science and Engineering, Massachusetts Institute of Technology, Cambridge, Massachusetts 02139

The relationship between the deposition conditions and the structural and electrical properties of *in situ* superconducting $YBa_2Cu_3O_{7-x}$ thin films deposited by off-axis magnetron sputtering has been investigated. High-quality films have been produced with a transition temperature T_C ($R=0$) of 92 K, a critical current density J_C (zero field) of 3.3×10^7 A/cm^2 at 4.2 K and 4.8×10^6 A/cm^2 at 77 K, and a microwave surface resistance R_S of 2.6×10^{-6} Ω at 1.5 GHz and 4.2 K which rises to 8.3×10^{-6} Ω at 77 K. Among the deposition conditions explored, substrate temperature was identified as the most influential in producing these high-quality films. A quantitative relationship was established between substrate temperature and T_C, normal-state resistivity ρ, J_C, orientation distribution, x-ray-diffraction peak broadening, lattice expansion, R_S, and penetration depth λ. Increasing substrate temperature results in an increase in T_C, a decrease in ρ, an increase in J_C, an increase in grain size, an increase in the ratio of c-axis- to a-axis-oriented grains, and a decrease in λ. The deposition conditions of high substrate temperature and oxygen pressure, used to form films of the highest electrical and structural quality, also promote the formation of CuO precipitates of about 1 μm in dimension, resulting from a slightly copper-rich stoichiometry.

I. INTRODUCTION

High-quality $YBa_2Cu_3O_{7-x}$ (YBCO) thin films have been prepared by a variety of techniques using both *in situ* and *ex situ* deposition methods. The first successful techniques to deposit YBCO thin films were *ex situ* methods, including coevaporation using metal-fluoride sources,[1] and chemical derivation of films from metalorganic liquid precursors.[2] *In situ* deposition techniques include pulsed laser deposition (laser ablation),[3,4] reactive evaporation,[5,6] molecular-beam epitaxy,[7,8] and sputtering.[9–11] These methods were initially advantageous over *ex situ* techniques because the overall processing temperature was lower. More recently, though, by postannealing in low oxygen pressures, the processing temperature for *ex situ* methods has been reduced to values similar to *in situ* techniques.[12–15] Therefore, a variety of both kinds of techniques can be used for producing high-quality films for electronics applications. To develop reproducible, manufacturable processes in order to fully exploit YBCO thin films for practical electronics applications, it is necessary to understand the relationship between the structural and electrical properties of the films and the processing conditions. In this article, we report on the relationship between substrate temperature and T_C, normal-state resistivity ρ, J_C, orientation distribution, x-ray-diffraction (XRD) peak broadening, lattice expansion, microwave surface resistance R_S, and penetration depth λ. Thin-film microstructure was inferred from XRD measurements and in some cases corroborated by scanning electron microscopy (SEM) and transmission electron microscopy (TEM).

II. EXPERIMENT

Superconducting thin films of YBCO were deposited *in situ* by off-axis rf magnetron sputtering.[16,17] The deposition chamber was an all-metal load-locked system pumped by a 1000 1/s turbo pump. The target was a 7.6-cm-diam pressed powder of stoichiometric superconducting YBCO[18,19] with a density of 5.986 g/cm^3. The target was annealed in oxygen at 440 °C prior to system installation and sputtered for a total of 23 h to condition it. The LaAlO$_3$ (100) substrates were thermally and mechanically anchored to a stainless-steel heater block using silver paste. This heater block was radiatively heated using a quartz lamp, and its temperature T_H controlled using a Chromel-Alumel thermocouple embedded into it. The actual substrate temperature T_S was calibrated as a function of T_H using 25-μm-diam Platinel thermocouple wires ultrasonically bonded to the substrate surface, a technique described in detail elsewhere.[20]

Films measuring about 2000 Å thick were deposited over a wide range of conditions by varying substrate temperature and oxygen pressure while holding total pressure constant at 160 mTorr and rf power constant at 125 W. Prior to depositing each film, the target was presputtered

[a] Also with: Department of Materials Science and Engineering, Massachusetts Institute of Technology, Cambridge, MA 02139; current address: Digital Equipment Corporation, Hudson, MA 01749.

for 1 h. After deposition, the oxygen pressure was raised at a rate of 2 Torr/min with the substrate temperature ramped to 400 °C in 20 min and held at this temperature for 1 h to oxygenate the film.

Structural properties of the resulting films were characterized using several techniques. X-ray diffraction was used to determine the phases present in the films and the crystallographic orientation both perpendicular to the surface and in plane. Two techniques were used: standard θ-2θ XRD and four-circle XRD, which is used to scan in θ, θ-2θ, chi, and phi. The θ-2θ measurements were performed using a Rigaku diffractometer and the four-circle measurements with a Huber goniometer. In both cases, Cu $K\alpha$ x-rays were generated from a rotating-anode source. The surface morphology of the films was investigated using SEM. Films were observed in plan view and cross section. Auger electron spectroscopy (AES) was used to measure film composition and uniformity and to identify secondary phases. The microstructure was characterized by cross-sectional and plan-view TEM and high-resolution electron microscopy (HREM). Electron-transparent specimens of the YBCO thin films were prepared by the usual multistep process involving sectioning, mechanical polishing, dimpling, and ion milling. The chemical analysis of secondary phases in these films was carried out by energy-dispersive spectroscopy (EDS) in a dedicated scanning transmission electron microscope (STEM).

The dc and rf electrical properties were also measured and correlated with structural properties and deposition conditions. Resistive transitions were measured using the standard four-point probe technique. Critical current density was measured by transport on 20-μm-wide, 2-mm-long patterned lines using a 5 μV/cm criterion. Surface resistance and penetration depth measurements were performed using a stripline resonator technique.[21] The dependence of the surface resistance on microwave current (power dependence) was also measured.[22] The resonator was constructed by patterning a 150-μm-wide, 2-cm-long transmission line coupled to input and output through a 750 μm gap. Films were patterned for J_C and R_S measurements by wet chemical etching using a dilute solution (0.25%) of phosphoric acid.

III. RESULTS

The YBCO thin films were deposited over a wide range of conditions by varying the heater temperature from 640 °C (T_S=625 °C) to 800 °C (T_S=765 °C) and by varying oxygen pressure $P(O_2)$ from 10 to 100 mTorr, as displayed in Fig. 1. The heater temperature T_H is controlled during deposition, and the calibrated substrate temperature T_S is used for characterizing the films. All deposition conditions resulted in the formation of in situ superconducting thin films. The results presented in this article are part of a larger investigation[17] which also included the effect of bombardment and changes in oxygen pressure during the low-temperature oxygenation step. The experiments summarized below focus on the influence of sub-
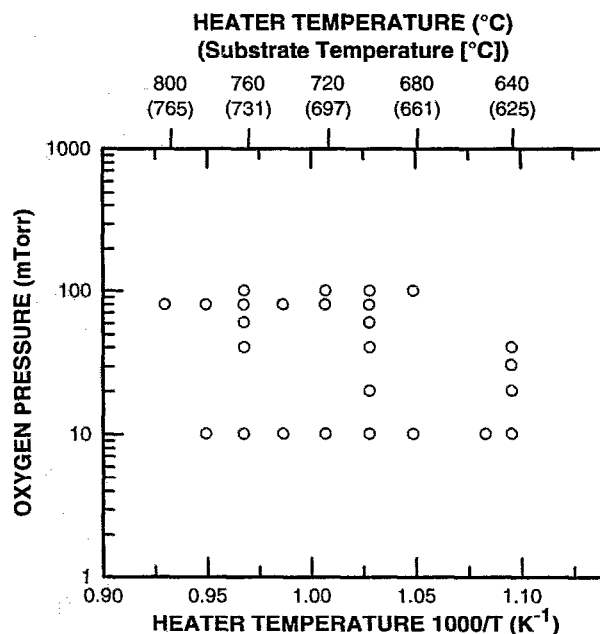

FIG. 1. Summary of deposition conditions used to deposit in situ superconducting YBCO thin films by single-target off-axis sputtering.

strate temperature in off-axis sputtering, which was identified as the most critical deposition parameter.

A. Electrical properties

The best electrical properties measured include a T_C of 92 K, a J_C of 3.3×10^7 A/cm^2 at 4.2 K and 4.8×10^6 A/cm^2 at 77 K, and a R_S for patterned films of 2.6×10^{-6} Ω at 1.5 GHz and 4.2 K and 8.5×10^{-5} Ω at 10 GHz, and 8.3×10^{-6} Ω at 1.5 GHz and 77 K and 2.0×10^{-4} at 10 GHz.[23] Deposition conditions which optimize these electrical properties are a high deposition temperature (T_S between 730 and 765 °C) and a high oxygen pressure [$P(O_2)=80$ mTorr].

The values of T_C, J_C, ρ, and R_S were systematically measured as a function of deposition temperature in a series of films deposited to correlate electrical and structural properties. Figure 2(a) shows ρ and J_C as a function of temperature for one of the best films of this series of experiments. This film was deposited at T_S=765 °C with $P(O_2)=80$ mTorr. The normal-state resistivity is low and the extrapolation of a linear fit to the ρ vs T curve between 150 and 250 K crosses the resistivity axis below zero. Figure 2(b) shows R_S as a function of temperature of the same film. The R_S in all the films in the series is higher than our best previously reported results,[23] but the changes in R_S and the other properties measured form a consistent set of results as discussed below. The $\rho(T)$ for films deposited at different temperatures with an oxygen pressure of 80 mTorr is shown in Fig. 3(a). The curves show metallic behavior in the normal state with a slight upward deviation near T_C, with resistivity increasing with decreasing deposition temperature. As deposition temperature is decreased, T_C ($R=0$) decreases and the extrapolated $\rho(0)$ intercept measured between 150 and 250 K at $T=0$ in-
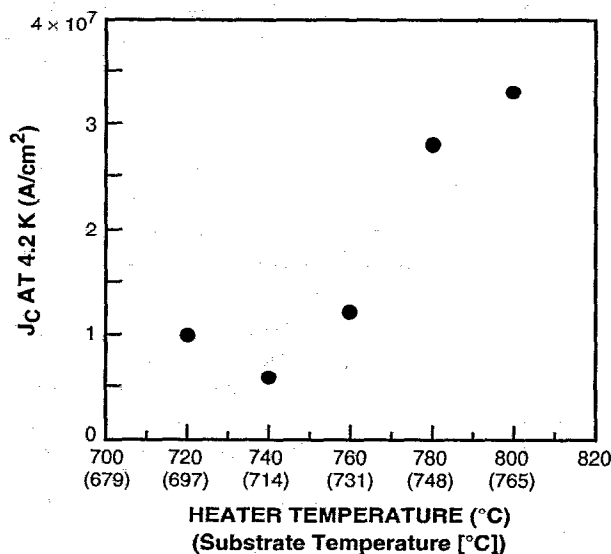
Westerheim et al.
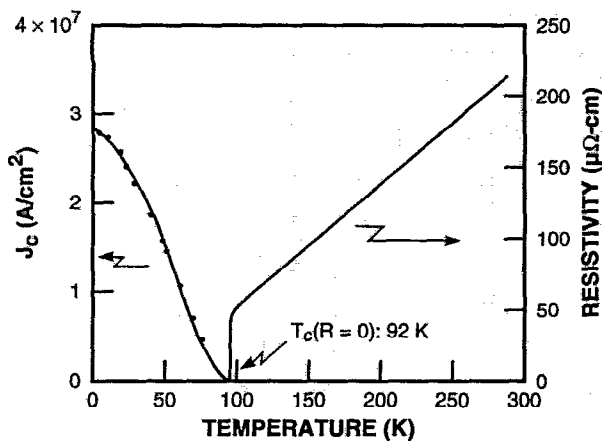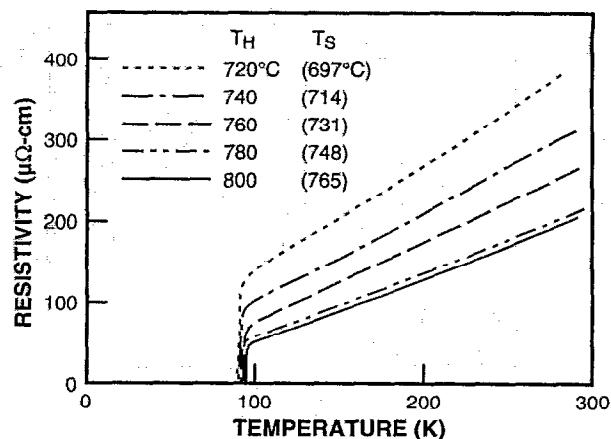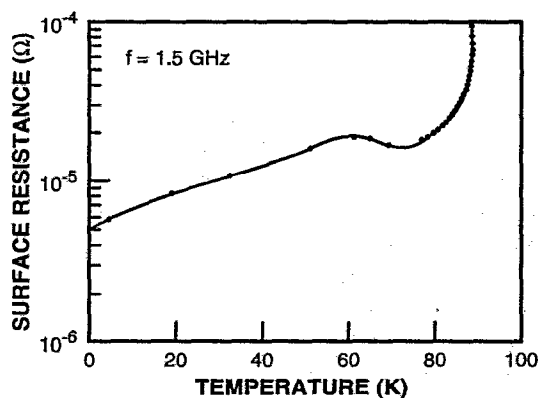
FIG. 2. dc and rf electrical properties as a function of temperature for a film deposited at $T_S = 765\,°C$ and $P(O_2) = 80$ mTorr. (a) Resistivity and critical current density. (b) Microwave surface resistance at 1.5 GHz.

FIG. 3. (a) Resistivity as a function of temperature for films deposited with different substrate temperatures. (b) Critical current density J_C as a function of deposition temperature.

creases. Critical current density also decreases with decreasing deposition temperature over this range as shown in Fig. 3(b). Figure 4 shows R_S at 1.5 GHz and 4.2 K as a function of rf current for the same series of films. Table I summarizes the dc properties and rf electrical properties of these films including R_S, λ, and power dependence. As deposition temperature increases, T_C and J_C increase, while ρ and λ decrease.

B. Structural properties

Standard $\theta - 2\theta$ XRD reveals that all the films are highly oriented with the c axis or a axis normal to the substrate. Figure 5 shows a diffraction pattern typical of the best films with 00l lines measured to 0013. This film was deposited at $T_S = 731\,°C$ with $P(O_2) = 80$ mTorr. No secondary phases are detected using this technique and the diffraction peaks are intense and narrow. Higher index peaks (>007) demonstrate the $K\alpha 1$-$K\alpha 2$ peak splitting that is typically observed in high-quality films. A phi scan of the {102} peaks in c-axis-oriented grains of a film grown under similar conditions is shown in Fig. 6 indicating that there are no misoriented grains in these films. The {102} peak was selected for this measurement instead of the more

intense {110} and {103} peaks because there are no overlapping substrate peaks. The splitting of the peaks is due to twinning in the a-b planes and this is the only observed defect. Figure 7(a) shows the peak splitting in greater detail. In addition, in the c-axis-oriented grains the {102} reflections from the film are offset from the {110} reflection in the substrate, indicating a deviation of about 0.4° between the $\langle 100 \rangle$ directions parallel to the film-substrate interface in the film and substrate. In contrast, the XRD pattern of a-axis grains in the same film, shown in Fig. 7(b), indicates that the $\langle 100 \rangle$ directions in the film and substrate are aligned.

As deposition temperature is decreased, several changes occur in the film microstructure. First, the c-axis lattice parameter increases from the bulk value 11.677 Å,[24] as shown in Fig. 8. This effect is more pronounced at low $P(O_2)$ than at high $P(O_2)$. Second, the diffraction peaks
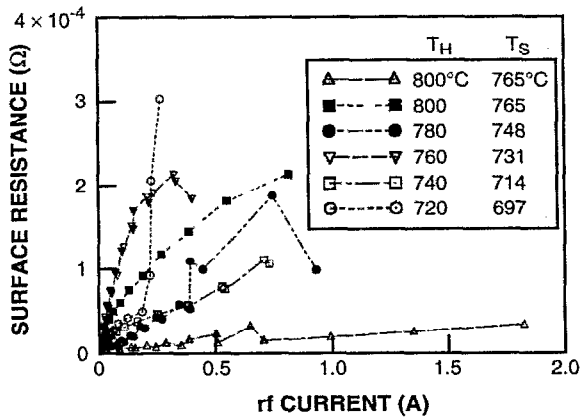
FIG. 4. Microwave surface resistance at 4 K and 1.5 GHz as a function of current for a series of films deposited at different temperatures. The values of R_S at low current are given in Table I. The variation of R_S with current among the films is substantially larger than the variation of low-current R_S.

FIG. 5. X-ray-diffraction pattern for a film deposited at $T_S = 731$ °C and $P(O_2) = 80$ mTorr.

broaden. This is illustrated in Fig. 9 which shows the full width at 50% maximum and 20% maximum of the 007 diffraction peaks for films deposited with an oxygen pressure of 80 mTorr. Finally, the orientation distribution of the film changes; as the deposition temperature is decreased, there is an increase in the component of a-axis-oriented grains. Figure 10(a) shows θ-2θ scans of 102 peaks measured in a-axis- and c-axis-oriented grains in 2200-Å-thick films deposited at the following T_S: 697, 714, 731, 748, and 765 °C. As deposition temperature decreases,
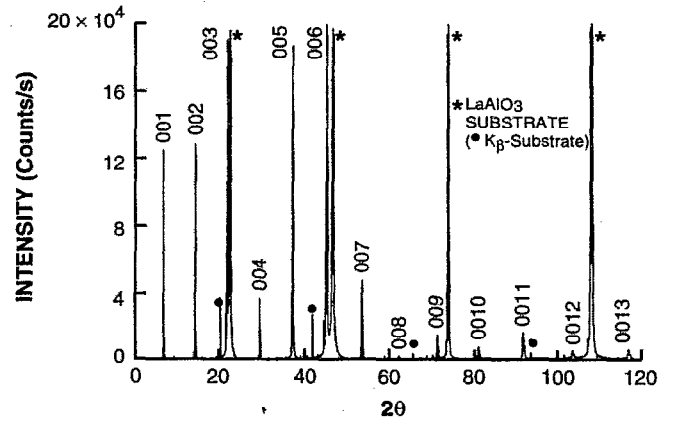
the c-axis peaks become less intense and the a-axis peaks become more intense. The orientation distribution, that is, the ratio of a-axis- to c-axis-oriented grains, is calculated by comparing the integrated diffracted intensities and correcting by a factor of 1.1 for the fact that (102) and (012) reflections are not resolved in θ-2θ, but are almost completely resolved in phi for the diffraction conditions used. The calculated orientation distribution of these films is plotted as a function of deposition temperature in Fig. 10(b).

All of the films deposited for R_S measurements had a mixed c-axis and a-axis orientation. At even lower deposi-

TABLE I. Summary of dc and rf electrical properties as a function of deposition temperature.

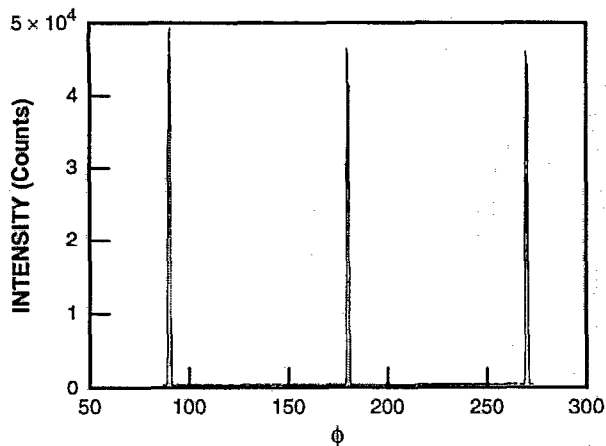| Deposition temperature		dc properties				rf properties				
T_H (°C)	T_S (°C)	T_C ($R=0$) (K)	ρ (300 K) ($\mu\Omega$ cm)	ρ (100 K) ($\mu\Omega$ cm)	J_C (4 K) (A/cm²)	f (GHz)	T (K)	R_S (Ω)	λ (μ)	Power dependence R_S at 0.25 A (Ω)
720	697	86.4	410	146	1.0×10^7	1.5	4.2	4.8×10^{-6}	0.3	2.1×10^{-4}
						1.5	77	6.0×10^{-5}		
						10	77	3.6×10^{-3}		
740	714	87.0	325	107	5.9×10^6	1.5	4.2	8.2×10^{-6}	0.22	4.7×10^{-5}
						1.5	77	3.75×10^{-5}		
						10	77	1.3×10^{-3}		
760	731	90.4	277	80	1.2×10^7	1.5	4.2	1.4×10^{-5}	0.2	2.0×10^{-4}
						1.5	72	5.0×10^{-5}		
						10	72	1.5×10^{-3}		
780	748	89.2	223	62	2.8×10^7	1.5	4.2		0.11	4.5×10^{-5}
						1.5	77	2.0×10^{-5}		
						10	77	6.0×10^{-4}		
800	765	89.7	217	61	3.3×10^7	1.5	4.2	1.25×10^{-5}	0.11	1.1×10^{-4}
						1.5	77	2.4×10^{-5}		
						10	77	1.0×10^{-3}		
800	765	92.2	216	55	2.85×10^7	1.5	4.2	5.4×10^{-6}	0.17	1.0×10^{-5}
						1.5	77	2.0×10^{-5}		
						10	77	3.5×10^{-4}		

FIG. 6. X-ray-diffraction phi scan of {102} peaks showing fourfold in-plane symmetry with no misoriented grains.
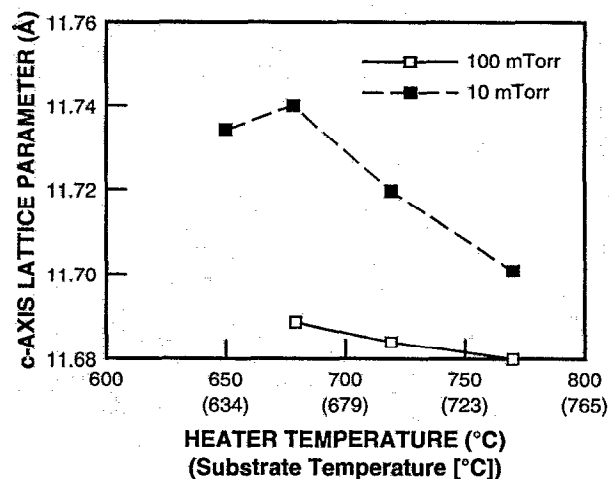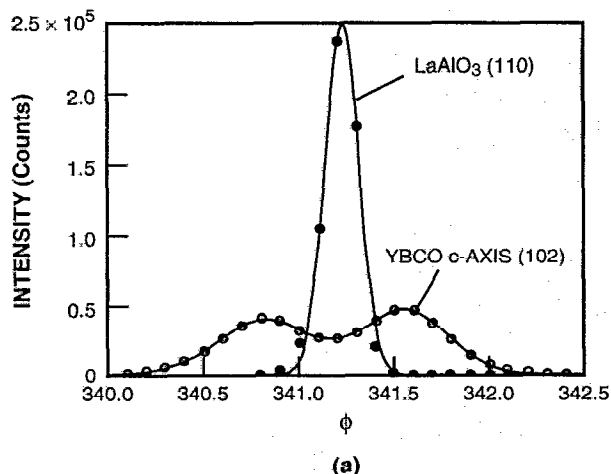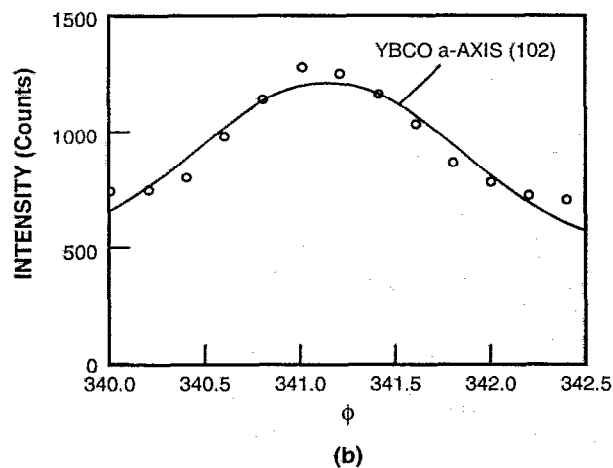

FIG. 8. The c-axis lattice expansion as a function of deposition temperature and oxygen pressure.

(a)

(b)

FIG. 7. X-ray-diffraction phi scan of a film with (a) c-axis-oriented grains and (b) a-axis-oriented grains. Also shown is the {110} peak of the LaAlO₃ substrate indicating the alignment between the film and substrate. Note that the relative positions of the peaks are of interest; the actual value of phi is arbitrary.

tion temperatures, the films become entirely a-axis oriented. Figure 11 shows a diffraction pattern of a film deposited at $T_S = 625$ °C with $P(O_2) = 20$ mTorr. This film is purely a-axis oriented. No 00l lines are detected and an intense 400 peak at 20 000 counts/s is clearly visible. Note that this diffraction pattern also exhibits artifact peaks from the substrate.

Changes in microstructure that can be inferred from XRD were in some cases also examined by SEM and TEM. Although XRD analysis suggests that the films are phase-pure YBCO, the SEM and TEM analysis indicates that this is not the case. Figure 12 shows plan-view and cross-sectional SEMs indicating that agglomerates visible on the film surface actually extend through the film thickness. Analysis of these precipitates by EDS, AES, and STEM reveals that most of them are polycrystalline CuO. The volume fraction of CuO in these films estimated from SEM analysis is up to 20%. The overall stoichiometry of all of the films is copper rich and slightly yttrium rich as mea-
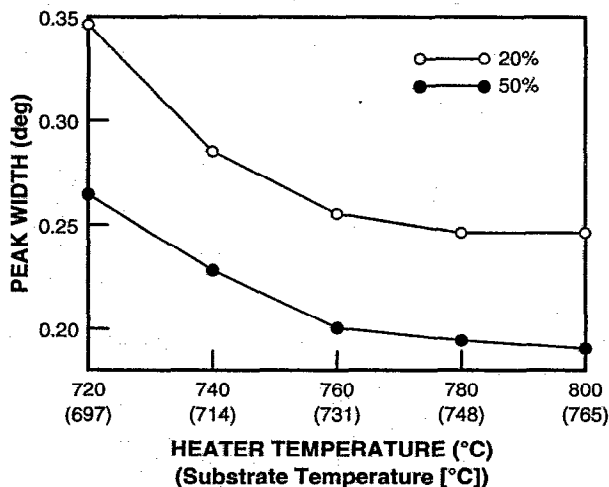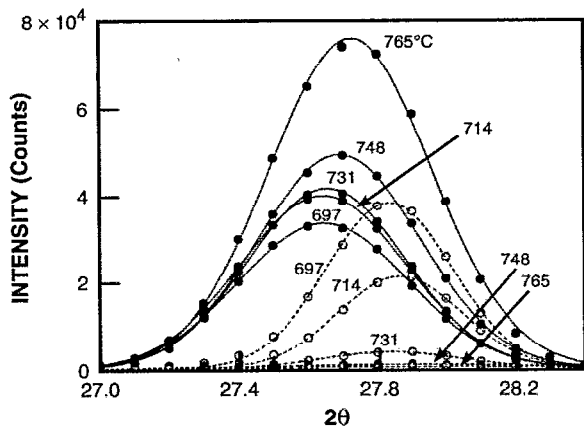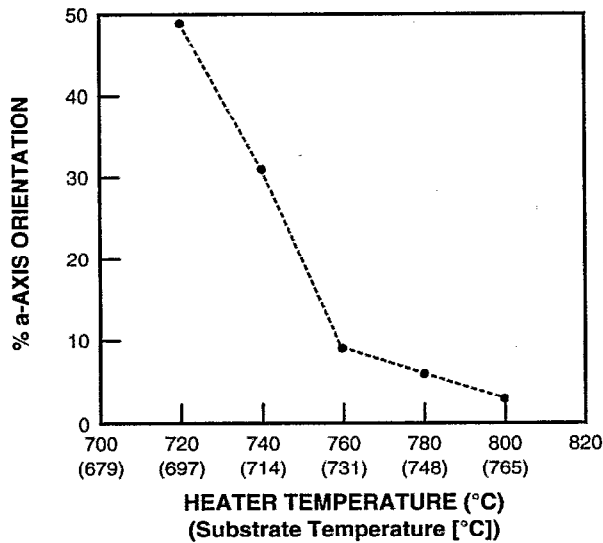

FIG. 9. The c-axis peak width broadening as a function of deposition temperature.

J. Appl. Phys., Vol. 75, No. 1, 1 January 1994

Westerheim et al.   397

(a)

(b)

FIG. 10. Four-circle x-ray-diffraction measurements of orientation distribution of films deposited at various temperatures. (a) θ-2θ scans of 102 peaks in a-axis (O) and c-axis (●) -oriented grains. The diffracted intensity increases for c-axis grains and decreases for a-axis grains with increasing deposition temperature in the series: T_S=697, 714, 731, 748, and 765 °C. (b) The a-axis component of the same films as a function of deposition temperature calculated from the curves in (a).
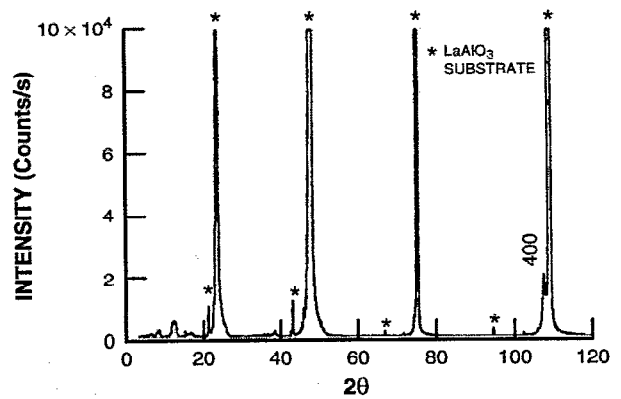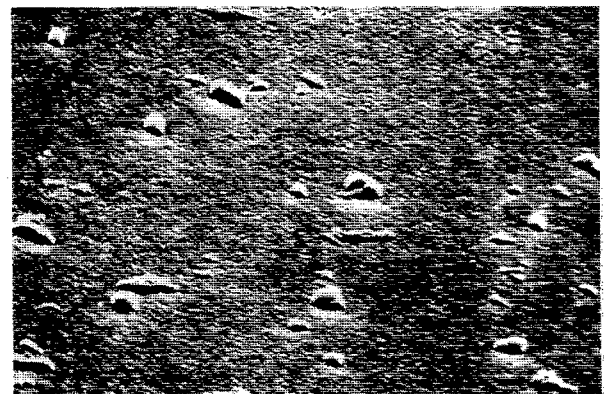

FIG. 11. X-ray-diffraction pattern of an a-axis-oriented YBCO film on a LaAlO$_3$ substrate.

oriented grains. The majority of the grain boundaries are oriented parallel to the (103) plane, which would result from impingement of two orthogonal a-axis grains along their faster growing b-axis direction. The figure also shows

(a)

(b)

FIG. 12. Scanning electron micrographs showing (a) CuO precipitates and (b) cross section of CuO precipitate extending through the entire film.

sured by AES. Other secondary phases have also been identified including Y$_2$O$_3$ and Cr-Ba oxide, measuring about 100 and 1000 Å in diameter, respectively, for films deposited at T_S=731 °C. The Cr-Ba oxide is caused by contamination from the oxidized stainless-steel heater block. Since this contamination was detected in some films, most of the films described in this investigation were deposited using heater blocks coated with Haynes 230, which does not contain chromium.

A plan-view HREM of a predominantly a-axis-oriented film is shown in Fig. 13(a). This film was deposited at T_S=679 °C and a low oxygen pressure, $P(O_2)$ = 10 mTorr. The figure clearly shows the presence of numerous 90° grain boundaries between the two variants of a-axis-
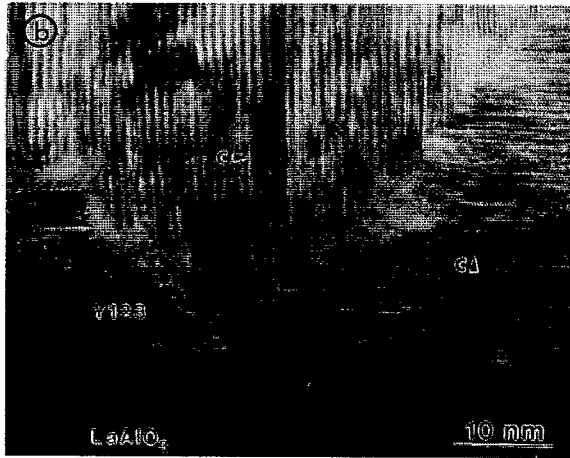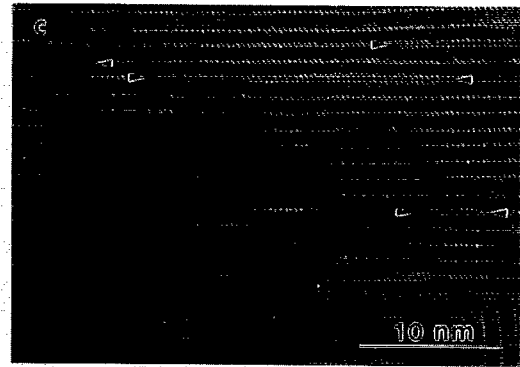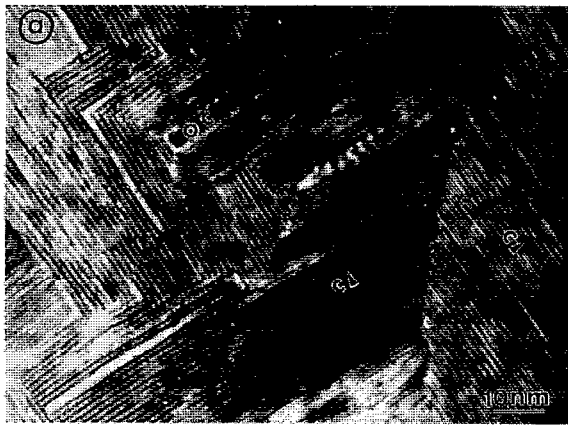
Westerheim *et al.*

FIG. 13. Transmission electron micrographs showing (a) plan view of a-axis grains, (b) cross section of an a-axis-oriented grain growing out of c-axis grains, and (c) stacking faults in the film in the form of extra Cu-O planes.

the presence of grain boundaries oriented parallel to the (010) planes due to the impingement of an a-axis grain growing along its faster-growing b-axis direction, on an orthogonal a-axis grain, growing along its slower c-axis direction. It should be noted that at this deposition temperature the film is still not completely a-axis oriented. A cross section of the film, presented in Fig. 13(b), shows that the film close to the interface is c-axis oriented, with an a-axis grain that has nucleated close to the film-substrate interface. In addition to grain boundaries, the film shows numerous stacking faults, mostly in the form of extra Cu-O planes, some examples of which are marked by arrows in Fig. 13(c). The microstructure and defects in these films will be discussed in detail elsewhere.[25]

IV. DISCUSSION

A consistent picture of the factors affecting film quality can be formed from the correlations between deposition conditions and measured properties of YBCO thin films. *In situ* superconducting films were achieved in all cases, and changes in deposition conditions led to systematic changes in the microstructure of the films which, in turn, affected electrical performance. The microstructure of the films, inferred from XRD measurements and in some cases confirmed by TEM, is considered first, since this is the property that is most fundamentally impacted by the deposition conditions. The resulting electrical properties are then discussed.

All films investigated were highly textured with c-axis, a-axis, or mixed c-axis and a-axis orientation. No secondary-phase peaks where observed in the θ-2θ XRD patterns of films even though secondary-phase precipitates were observed by SEM, AES, EDS, and TEM. Since these secondary phases are randomly oriented, their diffracted intensity is reduced by roughly a factor of 1000 and is not detected by XRD.[26-28] The expected diffracted intensity from an unoriented secondary phase is well within the background noise level for diffracted intensity, assuming a typical diffracted intensity of 1.5×10^5 cps for the most intense film peaks of a 2000-Å-thick c-axis-oriented film and estimating a 20% volume fraction of secondary phases.

Four-circle XRD reveals that the films exhibit fourfold in-plane symmetry, which is expected for growth on $LaAlO_3$, a pseudocubic substrate.[29] There are no 45° in-plane misoriented grains which are commonly observed in YBCO films on MgO.[30] The four-circle XRD measurements also reveal that the c-axis-oriented grains are twinned in the a-b plane and that the epitaxial registry between the film and the substrate for c-axis-oriented grains occurs along the $\langle 110 \rangle$ directions and not along $\langle 100 \rangle$ directions as commonly assumed. Figure 14 shows a highly exaggerated view of the two epitaxial orientations of a c-axis-oriented YBCO film twinned along {110} planes. This alignment has been previously demonstrated by Budai, Feenstra, and Boatner[31] in YBCO films prepared by

J. Appl. Phys., Vol. 75, No. 1, 1 January 1994
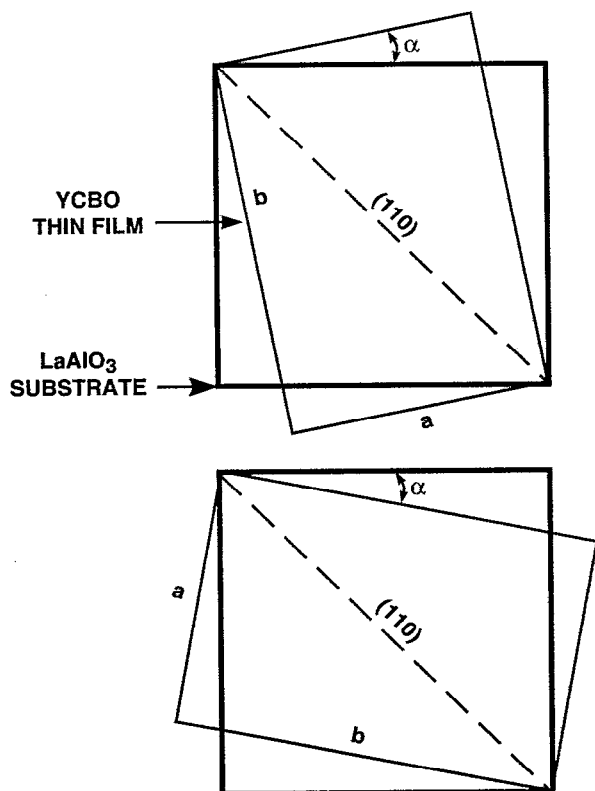
Westerheim *et al.* 399

FIG. 14. Exaggerated view of a twinned YBCO film showing film-substrate epitaxial registry.

coevaporation followed by a postdeposition anneal on $SrTiO_3$ and $KTaO_3$ substrates, but has not been widely investigated. Peak splitting in {102} phi scans has also been observed by Heidelbach et al.[32] in YBCO films deposited by laser ablation.

A simple calculation based on bulk lattice parameters for YBCO ($a = 3.822$ Å, $b = 3.891$ Å, and $c = 11.677$ Å)[24] and on the assumption that the film and substrate are perfectly registered along the $\langle 110 \rangle$ direction yields an angular difference between the film and substrate $\langle 100 \rangle$ directions of 0.5°, which is consistent with the measured value of about 0.4°. Analysis of the mismatch between the YBCO film and the $LaAlO_3$ substrate ($a = 3.790$ Å)[29] based on room-temperature lattice constants can explain this observation. While the lattice mismatch along the [100] direction is quite small, 0.79%, the mismatch along the [010] direction is much larger, 2.37%. The mismatch along the $\langle 110 \rangle$ direction is 1.47%. Since strain energy is proportional to the square of the misfit, it is energetically favorable for the film and the substrate to be matched along the $\langle 110 \rangle$ direction.

Fourfold in-plane symmetry of the diffraction pattern for c-axis-oriented grains is the result of twinning in the a-b plane as discussed above. Fourfold in-plane symmetry is also observed in a-axis-oriented grains, but this is caused by a twofold degeneracy in the possible orientations of the c axis with respect to the substrate. In contrast to c-axis-oriented grains, the [010] and [001] directions in a-axis-

oriented grains are aligned with respect to the substrate $\langle 100 \rangle$ directions. Furthermore, the fact that no b-axis-oriented grains are observed indicates that the a-axis-oriented grains are not twinned, which has also been shown for ex situ films.[31] This is to be expected because when the film undergoes the tetragonal to orthorhombic transition during cooling, the lattice expansion along the b axis is smaller than the contraction along the a axis, as indicated by the lattice parameter measurements by Specht et al.[33] Thus, minimization of strain energy favors the b axis lying in plane and the film being a-axis oriented.

The observed increase in XRD peak width with decreasing deposition temperature, shown in Fig. 9, is consistent with the expected decrease in grain size with decreasing deposition temperature, with peak width inversely proportional to grain size.[27,34] The change in grain size is a result of a decrease in grain growth with decreased atomic mobility, and an increase in nucleation rate from an increase in thermodynamic driving force.[35,36] The exact change in grain size cannot, however, be uniquely determined since film disorder is also expected to increase with decreasing deposition temperature. Several types of disorder may be present in the films. It may be in the form of cation disorder whereby Ba replaces Y on the YBCO lattice as proposed by Michikami, Asahi, and Asano,[37] and Matijasevic et al.,[38] defects on the oxygen sublattice, or other defects such as intercalation of excess Cu-O planes as observed by TEM in this investigation. Grain size and defects in these films will be discussed in detail elsewhere.[25]

The change in orientation from c axis at high deposition temperatures to a axis at low deposition temperatures shown in Fig. 10(b) has been observed previously.[32,39,40] Inam et al.[39] have measured ion-channeling yield as a function of deposition temperature for PrBaCuO films as orientation changes from c axis to a axis, and Heidelbach et al.[32] used four-circle XRD to measure relative amounts of a-axis and c-axis-oriented grains in laser-deposited films. Eom et al.[40] were the first to observe predominantly a-axis-oriented films on $SrTiO_3$ substrates. They attributed the change in film orientation to a competition between minimization of surface energy which promotes c-axis-oriented growth (as supported by observations of growth rate anisotropy in YBCO) and minimization of lattice misfit energy between the substrate and the film which promotes a-axis-oriented growth. Unlike the case with $SrTiO_3$, for films deposited on $LaAlO_3$ substrates the misfit minimization alone would favor the a-axis lying in plane, so that a-axis-oriented films should not form. The formation of a-axis orientation may then be favored at low deposition temperatures because of reduced atomic mobility to form the layered structure. The ion-channeling work by Inam et al.[39] indicates that almost pure a-axis-oriented films have a higher degree of crystallographic perfection than films of mixed orientation grown at slightly higher temperatures; films become increasingly disordered with decreasing deposition temperature until the a-axis orientation is formed. The formation of pure a-axis-oriented films in this work is significant in that it may indicate that a-axis YBCO can nucleate at the growth interface which would challenge

Westerheim et al.

the model of c-axis orientation always forming first in a thin layer at the growth interface.[32,41]

The CuO precipitates measuring up to 1 μm in diameter and extending through the entire film thickness have been widely observed in YBCO thin films. These agglomerates did not directly degrade the electrical performance of the films. In fact, the substrate temperature and oxygen pressure combinations which promoted the best electrical and structural properties in this investigation also resulted in the largest CuO precipitates. However, this surface roughness is obviously a problem for film patterning, for fabrication of small features, and for deposition of multilayered structures.

The formation of CuO secondary phases is consistent with the observation that these films are copper rich, even though they are deposited from a single stoichiometric target. The films may be copper rich for several reasons, such as: a difference in scattering of cations in the gas phase resulting from mass differences; a difference in initial kinetic energy of cations as they are ejected from the target again resulting from mass differences; or a difference in cation sticking coefficients on YBCO. The exact mechanism is not known. Excess copper is rejected from the structure since, for a given temperature and oxygen pressure, YBCO is a line compound in composition space.

The formation of CuO precipitates must be accompanied by significant amounts of copper surface diffusion. The formation of the CuO precipitates may then be thought of as an indicator of the level of adatom mobility during film deposition. On the assumption that composition is constant, the same conditions which lead to large secondary-phase precipitates also contribute to improved structure and electrical properties. At low deposition temperatures, excess copper may lead to defects in Cu-O planes, increasing film disorder. We have recently used externally applied magnetic fields to alter plasma conditions and bombardment, thus changing the copper content of the films and improving surface morphology.[17,42,43]

Changes in the structural properties discussed above can be correlated with changes in electrical properties. We found that among the deposition conditions explored in this investigation the substrate temperature is also the most significant factor affecting the electrical properties of YBCO films. As substrate temperature is increased, T_C and J_C increase, while normal-state resistivity $\rho(T)$ and the $T=0$ resistivity intercept $\rho(0)$ decrease. These parameters were shown to follow a clear and systematic trend as a function of deposition temperature, as summarized in Table I. Microwave surface resistance R_S did not follow any apparent trend, but the penetration depth λ was shown to increase with decreasing deposition temperature. As mentioned earlier, this series of films exhibited higher R_S values than previously reported, indicating that some unidentified factor may be contributing to the surface resistance. However, all the other film properties are consistent with the previous discussion.

A simple analysis of the normal-state resistivity as a function of temperature gives insight to the relationship between microstructure and microscopic transport of current in these films, whereby overall resistivity is determined by resistivity from grain boundaries and the intrinsic resistivity of weak-link-free crystals.[44] The increase in ρ with decreasing deposition temperature may then be seen as the result of two factors: decreasing grain size, which increases the number of grain boundaries intersecting a conduction path, and increasing intragrain disorder possibly due to cation disorder or defects in Cu-O planes. An increase in cation disorder in the film should also lead to a suppression of T_C at lower deposition temperatures, which is consistent with our experimental observations. The even larger resistivities measured in a-axis-oriented films can be explained by the fact that microscopic current paths along a-b planes are intersected by many 90° grain boundaries.

The decrease in J_C with decreasing deposition temperature may also be understood by changes in microstructure, whereby J_C is determined by critical currents for intergrain Josephson junctions, intragrain junctions, and pinning.[44] Different defects in the YBCO thin films play competing roles; grain boundaries serve as weak links which decrease J_C, and other types of defects create pinning sites which increase J_C.

As deposition temperature decreases, the decrease in grain size leads to more grain boundaries intersecting a current path which can explain the reduction in J_C, although Chan et al.[45] have shown that not all 90° angle grain boundaries degrade J_C. Kromann et al.[46] have found a 70% reduction in J_C by increasing the amount of a-axis-oriented grains in YBCO films from 0.6% to 8.3%, although we have measured a J_C as high as 1×10^7 A/cm^2 at 4.2 K in a predominantly a-axis-oriented film deposited at $T_S = 697$ °C. This suggests that grain orientation may play a secondary role to grain size.

The very large critical currents measured, in the mid 10^7 A/cm^2 range, require a high degree of pinning. At present, the source of pinning in YBCO thin films has not been identified, but many candidates exist including coherent secondary-phase precipitates[47,48] such as Y_2O_3, twin boundaries,[49] dislocations,[50] screw dislocations in the center of growth spirals,[51,52] and oxygen vacancies.[53] However, none of these defects supply the amount of pinning necessary to explain the large critical currents.

Microwave surface resistance does not appear to follow the trends established for the change in T_C, J_C, and resistivity. In ideal superconductors the low-power surface resistance results from microwave losses from the resistance produced by unpaired electrons. The two-fluid model[54] can be used to calculate R_S as a function of the density of paired and unpaired electrons, the mobility of these electrons, and λ, but comparison with measurements shows that other phenomena must be added to the two-fluid model. Hylton and Beasley[55] introduced the concept of the material being a network of grains coupled by weak links. A recently formulated coupled-grain model[56] extends the ideas of Hylton and Beasley[55] to include the power dependence and can be used to gain some insight into the behavior of the surface resistance at low power and as a function of the power. In the coupled-grain model the YBCO is represented by a network of ideal superconducting grains

coupled together by Josephson-junction-like weak links which can arise from a variety of defects including grain boundaries. The power dependence of R_S results from the variation of the inductance of the Josephson-junction weak links with rf current. The surface resistance depends on both the quality and the number of the weak links. The quality of the weak links is determined by a critical current (not necessarily the same as the J_C measured by transport since at low frequencies the weak links are shunted by other parallel paths in the film) and by the leakage resistance for the links. Deposition temperature affects both the number and quality of the weak links. Although the power dependence of R_S is not uniquely determined by the deposition temperature in these experiments, it is a clear trend that higher deposition temperatures yield lower power dependence. The low-power surface resistance R_S, however, is not clearly correlated with deposition temperature. Thus, the improvement of power dependence with increasing deposition temperature can be identified with weak links of higher critical current, while the independence of the low-field R_S indicates strongly that the film microstructure is influenced by other factors, such as substrate ion bombardment or substrate preparation, which were not as tightly controlled as the substrate temperature in this series of experiments.

V. SUMMARY AND CONCLUSIONS

In situ superconducting YBCO thin films were formed over a wide range of processing conditions. Structural and electrical properties were correlated with deposition temperature. All films exhibited *c*-axis, *a*-axis, or mixed *c*-axis and *a*-axis orientation and the distribution of these orientations was quantified as a function of deposition temperature. The films had two different orientations in plane, with ⟨110⟩ directions aligned between the film and the substrate in *c*-axis-oriented grains, and ⟨100⟩ directions aligned in the plane of the film-substrate interface in *a*-axis-oriented grains. Precipitates of CuO, Cr-Ba oxide, and Y_2O_3 were identified in the films but these defects do not necessarily degrade electrical properties. The best films had a T_C ($R=0$) of 92 K, a J_C (zero field) of 3.3×10^7 A/cm^2 at 4.2 K and 4.8×10^6 A/cm^2 at 77 K, and a R_S of 2.6×10^{-6} Ω at 1.5 GHz and 4.2 K which rises to 8.3×10^{-6} Ω at 77 K. Decreasing substrate temperature resulted in a decrease in T_C, an increase in ρ, a decrease in J_C, a decrease in grain size, an increase in the ratio of *a*-axis- to *c*-axis-oriented grains, and an increase in λ. The low-power R_S did not correlate with deposition temperature, but the power dependence of R_S was shown to increase with decreasing deposition temperature.

[1] P. M. Mankiewich, J. H. Scofield, W. J. Skocpol, R. E. Howard, A. H. Dayem, and E. Good, Appl. Phys. Lett. **51**, 1753 (1987).

[2] P. C. McIntyre, M. J. Cima, and M. F. Ng, J. Appl. Phys. **68**, 4183 (1990).

[3] T. Venkatesan, X. D. Wu, B. Dutta, A. Inam, M. S. Hegde, D. M. Hwang, C. C. Chang, L. Nazar, and B. Wilkens, Appl. Phys. Lett. **54**, 581 (1989).

[4] G. Koren, A. Gupta, R. J. Baseman, M. I. Lutwyche, and R. B. Laibowitz, Appl. Phys. Lett. **55**, 2450 (1989).

[5] T. Terashima, Y. Bando, K. Iijima, K. Yamamoto, and K. Hirata, Appl. Phys. Lett. **53**, 2232 (1988).

[6] N. Missert, R. Hammond, J. E. Mooij, V. Matijasevic, P. Rosenthal, T. H. Geballe, A. Kapitulnik, M. R. Beasley, S. S. Laderman, C. Lu, E. Garwin, and R. Barton, IEEE Trans. Magn. **25**, 2418 (1989).

[7] J. S. Harris, J. N. Eckstein, E. S. Hellman, and D. G. Schlom, J. Cryst. Growth **95**, 607 (1989).

[8] J. Kwo, M. Hong, D. J. Trevor, R. M. Fleming, A. E. White, R. C. Farrow, A. R. Kortan, and K. T. Short, Appl. Phys. Lett. **53**, 2683 (1988).

[9] R. L. Sandstrom, W. J. Gallagher, T. R. Dinger, R. H. Koch, R. B. Laibowitz, A. W. Kleinsasser, R. J. Gambino, B. Bumble, and M. F. Chisolm, Appl. Phys. Lett. **53**, 444 (1988).

[10] C. B. Eom, J. Z. Sun, K. Yamamoto, A. F. Marshall, K. E. Luther, T. H. Geballe, and S. S. Laderman, Appl. Phys. Lett. **55**, 595 (1989).

[11] M. R. Hahn, T. L. Hylton, K. Char, M. R. Beasley, and A. Kapitulnik, J. Vac. Sci. Technol. A **10**, 82 (1991).

[12] R. Feenstra, T. B. Lindemer, J. D. Budai, and M. D. Galloway, J. Appl. Phys. **69**, 6569 (1991).

[13] M. P. Siegal, S. Y. Hou, J. M. Phillips, T. H. Tiefel, and J. H. Marshall, J. Mater. Res. **7**, 2658 (1992).

[14] A. Mogro-Campero and L. G. Turner, Appl. Phys. Lett. **58**, 417 (1991).

[15] P. C. McIntyre, M. J. Cima, J. A. Smith, Jr., R. B. Hallock, M. P. Siegal, and J. M. Phillips, J. Appl. Phys. **71**, 1868 (1992).

[16] A. C. Westerheim, L. S. Yu-Jahnes, and A. C. Anderson, IEEE Trans. Magn. **27**, 1001 (1991).

[17] A. C. Westerheim, Ph.D. thesis, MIT, 1992.

[18] Tosoh SMD, Inc., Grove City, OH.

[19] Superconductive Components, Inc., Columbus, OH.

[20] A. C. Westerheim, A. C. Anderson, and M. J. Cima, Rev. Sci. Instrum. **63**, 2282 (1992).

[21] D. E. Oates, A. C. Anderson, and P. M. Mankiewich, J. Supercond. **3**, 251 (1990).

[22] D. E. Oates, P. P. Nguyen, G. D. Dresselhaus, M. S. Dresselhaus, C. W. Lam, and S. M. Ali, J. Supercond. **5**, 361 (1992).

[23] D. E. Oates and Alfredo C. Anderson, IEEE Trans. Magn. **27**, 867 (1991).

[24] R. J. Cava, B. Batlogg, C. H. Chen, E. A. Rietman, S. M. Zahurak, and D. Werder, Phys. Rev. B **36**, 5719 (1987).

[25] D. Bhatt, S. N. Basu, A. C. Westerheim, and Alfredo C. Anderson (unpublished).

[26] L. Alexander, H. P. Klug, and E. Kummer, J. Appl. Phys. **19**, 742 (1948).

[27] B. D. Cullity, *Elements of X-Ray Diffraction* (Addison-Wesley, Reading MA, 1978).

[28] J. Sizemore, R. Barton, A. Marshall, J. C. Bravman, M. Naito, and K. Char, IEEE Trans. Magn. **MAG-25**, 2245 (1989).

[29] S. Geller and V. B. Bala, Acta Crystallogr. **9**, 1019 (1956).

[30] S. McKernan, M. G. Norton, and C. B. Carter, J. Mater. Res. **7**, 1052 (1992).

[31] J. D. Budai, R. Feenstra, and L. A. Boatner, Phys. Rev. B **39**, 12355 (1989).

[32] F. Heidelbach, H.-R. Wenk, R. E. Muenchausen, S. Foltyn, N. Nogar, and A. D. Rollett, J. Mater. Res. **7**, 549 (1992).

[33] E. D. Specht, C. J. Sparks, A. G. Dhere, J. Brynestad, O. B. Cavin, D. M. Kroeger, and H. A. Oye, Phys. Rev. B **37**, 7426 (1988).

[34] S. Mader, in *Handbook of Thin Film Technology*, edited by L. I. Maissel and R. Glang (McGraw-Hill, New York, 1970).

[35] H. J. Frost and C. V. Thompson, Acta Metall. **35**, 529 (1987).

402   J. Appl. Phys., Vol. 75, No. 1, 1 January 1994

Westerheim *et al.*

[36] E. N. Gilbert, Ann. Math. Stat. **33**, 958 (1962).

[37] O. Michikami, M. Asahi, and H. Asano, Jpn. J. Appl. Phys. **28**, L448 (1989).

[38] V. Matijasevic, P. Rosenthal, K. Shinolara, A. F. Marshall, R. H. Hammond, and M. R. Beasley, J. Mater. Res. **6**, 682 (1991).

[39] A. Inam, C. T. Rogers, R. Ramesh, K. Remschnig, L. Farrow, D. Hart, T. Venkatesan, and B. Wilkens, Appl. Phys. Lett. **57**, 2484 (1990).

[40] C. B. Eom, A. F. Marshall, S. S. Laderman, R. D. Jacowitz, and T. H. Geballe, Science **249**, 1549 (1990).

[41] S. N. Basu, A. H. Carim, and T. E. Mitchell, J. Mater. Res. **6**, 1823 (1991).

[42] A. C. Westerheim, P. C. McIntyre, S. N. Basu, D. Bhatt, L. S. Yu-Jahnes, A. C. Anderson, and M. J. Cima, J. Electron. Mater. **22**, 1113 (1993).

[43] A. C. Anderson, presented at the Materials Research Society Fall Symposium, 30 Nov.–4 Dec. 1992.

[44] J. Halbritter, Int. J. Mod. Phys. B **3**, 719 (1989).

[45] S. W. Chan, D. M. Hwang, R. Ramesh, S. M. Sampere, L. Nazar, R. Gerhardt, and P. Pruna, in *High T_c Superconducting Thin Films: Processing, Characterization and Applications*, edited by R. L. Stockbauer, S. V. Krishnaswamy, and R. C. Kurtz (American Institute of Physics, New York, 1990), p. 172.

[46] R. Kromann, J. B. Bilde-Sørensen, R. de Reus, N. H. Andersen, P. Vase, and T. Freltoft, J. Appl. Phys. **71**, 3419 (1992).

[47] S. Jin, T. H. Tiefel, and G. W. Kammlott, Appl. Phys. Lett. **59**, 540 (1991).

[48] U. Poppe, N. Klein, U. Dähne, H. Soltner, C. L. Jia, B. Kabius, K. Urban, A. Lubig, K. Schmidt, S. Hensen, S. Orbach, G. Müller, and H. Piel, J. Appl. Phys. **71**, 5572 (1992).

[49] B. M. Lairson, S. K. Streiffer, and J. C. Bravman, Phys. Rev. B **42**, 10 067 (1990).

[50] S. Jin, G. W. Kammlott, S. Nakahara, T. H. Tiefel, and J. E. Graebner, Science **253**, 427 (1991).

[51] M. Hawley, I. D. Raistrick, J. G. Beery, and R. J. Houlton, Science **251**, 1587 (1991).

[52] C. Gerber, D. Anselmetti, J. G. Bednorz, J. Mannhart, and D. G. Schlom, Nature **350**, 279 (1991).

[53] R. Feenstra, D. K. Christen, C. E. Klabunde, and J. D. Budai, Phys. Rev. B **45**, 7555 (1991).

[54] T. P. Orlando and K. A. Delin, *Foundations of Applied Superconductivity* (Addison-Wesley, Reading, MA, 1991).

[55] T. L. Hylton and M. R. Beasley, Phys. Rev. B **39**, 9042 (1989).

[56] P. P. Nguyen, D. E. Oates, G. D. Dresselhaus, and M. S. Dresselhaus, Phys. Rev. B **48**, 6400 (1993).

J. Appl. Phys., Vol. 75, No. 1, 1 January 1994

Westerheim *et al.* 403